



室蘭工業大学

学術資源アーカイブ

Muroran Institute of Technology Academic Resources Archive



Function-expansion-based topology optimization of three-dimensional optical waveguide devices with multi-layered structure considering layer thickness

メタデータ	言語: English 出版者: ELSEVIER 公開日: 2020-12-23 キーワード (Ja): キーワード (En): Topology optimization, Function expansion method, Finite element method (FEM), Optical waveguide device 作成者: TOMIOKA, Shun, IGUCHI, Akito, TSUJI, Yasuhide メールアドレス: 所属:
URL	http://hdl.handle.net/10258/00010347

This work is licensed under a Creative Commons Attribution-NonCommercial-ShareAlike 4.0 International License.



Function-Expansion-Based Topology Optimization of Three-Dimensional Optical Waveguide Devices with Multi-Layered Structure Considering Layer Thickness

Shun Tomioka, Akito Iguchi, Yasuhide Tsuji*

The Division of Information and Electronic Engineering, Muroran Institute of Technology, Muroran, 050-8585 Japan

Abstract

So far, an optimal design method for 2D and 3D design of optical waveguide devices topology optimization based on a function expansion method has been reported. In this paper, we improve the conventional function-expansion-based topology optimization method to design three-dimensional photonic devices with structural variation in the depth direction. In order to design realistic 3D optical waveguide devices, we consider a layered structure and design each layer by using function-expansion-based topology optimization method. In this approach, undesired floating structures are avoided and layer thickness can be optimized. The validity of this method is verified through design examples of a polarization splitter and rotator (PSR) and a crossing waveguide which have two-layer structure.

Keywords: Topology optimization, Function expansion method, Finite element method(FEM), Optical waveguide device

1. Introduction

Due to the spread of the Internet and smartphones, communication traffic is increasing, and high speed and large capacity optical communication systems are more and more required. In order to respond to such demands, it is indispensable to develop higher performance compact photonic devices, and the related researches are actively conducted. Especially, silicon nanophotonics has great possibility to realize such devices, and extensive researches on these devices are being carried out.

Recently, topology optimization methods have begun to be used to realize high-performance optical waveguide devices [1–8]. In the topology optimization, we can find out optimum structures that realize desired characteristics without any past experience and knowledge. The topology optimal design method of photonic devices using function expansion method for structural representation has been also proposed [9–13]. The function expansion method has advantages that it allows design with a high degree of freedom using a small number of design variables and it can easily suppress gray area which is an intermediate material region artificially arranged in the ordinal sensitivity analysis.

In order to realize high-performance optical waveguide devices with smaller footprint, it has been shown that utilizing an asymmetric structure along the depth direction is an effective way [14–18]. The waveguide devices in [14]

achieves high performance operation within a small footprint and the polarization rotator (PR) shown in [15] cannot be essentially realized unless the structural asymmetry in the depth direction is utilized. In [19], the function-expansion-based topology optimization for layered three-dimensional optical waveguide devices has been proposed. However, the obtained device structure by this approach has some undesired floating structure. Moreover, layer thickness is fixed before in-plane optimization and cannot be optimized.

In this paper, in order to make it possible to design three dimensional optical waveguide devices with layered structure along depth direction by using function-expansion-based topology optimization, we make several improvements to the conventional one. First, we divide a design region into a few layers, and independently express the material distribution within each layer. At that time, in order to avoid floating structures which do not have support underneath them, we apply appropriate constraint to the structure definition function. In addition, in order to simplify an optimized device structure, we introduce a structural smoothing filter. Moreover, in this design approach, we improve the conventional approach to be able to optimize not only in-plane structures but also layer thicknesses.

We verify the effectiveness of the proposed approach through design examples of optical waveguide devices with asymmetric structure in the depth direction. In Section 2, we illustrate the proposed design approach. A few numerical results are shown in Section 3 and the conclusion is given in Section 4.

*Corresponding author.

Email address: y-tsuji@mmm.muroran-it.ac.jp (Yasuhide Tsuji)

2. Topology optimization method for photonic devices with layered structure

2.1. Representation of refractive index distribution for layered structure by function-expansion method

Considering an optical waveguide device as shown in Fig. 1, and assuming the light is launched into the port 1, we consider the problem to optimize the refractive index profile that can realize the desired transmission characteristics.

In order to express a layered structure, we have extended the function expansion method [9] and have expressed the refractive index distribution as follows:

$$n_i^2(x, y, z) = n_a^2 + (n_b^2 - n_a^2)H(w_i(x, z)) \quad (1)$$

$$w_i(x, z) = \sum_{j=1}^N c_j^{(i)} f_j(x, z) \quad (i = 1, 2, 3 \dots) \quad (2)$$

where n_i is the refractive index distribution in the i -th layer and the function $H(w_i)$ is used to binarize a continuous value of $w_i(x, z)$ into either 0 or 1. Where n_a and n_b ($n_a < n_b$) are the refractive indices of two considered materials, respectively. In order to enable a sensitivity analysis described in Section 2.3, the refractive index distribution $n_i(x, y, z)$ has to be defined as a continuous function. In this work, we employ a modified Heaviside function with transition region as $H(w_i)$ [9].

The function $w_i(x, z)$ which determines the geometry of the i -th layer is independently optimized in each layer like Fig. 2. In this expression, the device structure is determined by the amplitude coefficient $c_j^{(i)}$ of each basis function given in each layer and these coefficients are the design variables in function expansion method. In this paper, Fourier series [11] is employed as a basis of structural definition function. This expression realize optimal design of photonic devices with asymmetric structure along the depth direction. However, since each layer is independently designed, floating structures may appear and such structures are difficult to fabricate.

In order to avoid floating structures, we revise (1) as the following expression:

$$n_i^2 = n_a^2 + (n_b^2 - n_a^2)L_i \quad (i = 1, 2, 3 \dots) \quad (3)$$

$$L_i = L_1 + \sum_{k=2}^i (1 - L_{k-1})H(w_k) \quad (i \geq 2) \quad (4)$$

$$L_1 = H(w_1). \quad (5)$$

The structure in i -th layer is given as an ORed structure of the structure defined by w_i and that in the upper layer. By using this expression, appearance of floating structure can be forbidden. In the case of two layered structure, (3) in each layer is expressed as follows:

$$n^2(x, y, z) = \begin{cases} n_a^2 + (n_b^2 - n_a^2)H(w_1) & \text{(upper layer)} \\ n_a^2 + (n_b^2 - n_a^2)H_{OR}(w_1, w_2) & \text{(lower layer)} \end{cases} \quad (6)$$

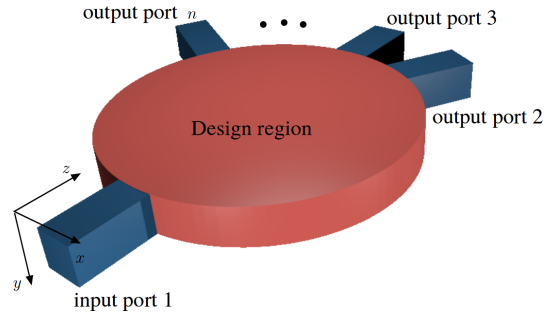


Figure 1: Optimization problem of 3D optical waveguide.

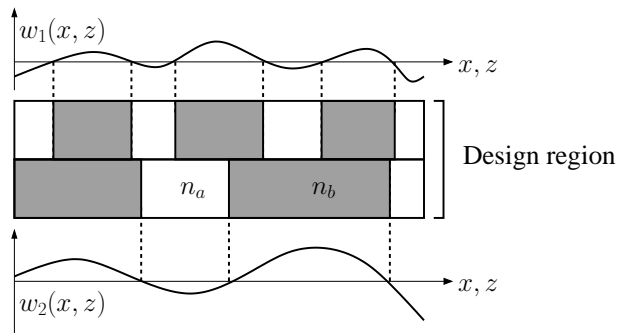


Figure 2: Representation of layered structure by function expansion method

$$H_{OR}(w_1, w_2) = H(w_1) + H(w_2) - H(w_1)H(w_2). \quad (7)$$

2.2. Full-vectorial finite element method of photonic devices

In order to analyze three-dimensional photonic devices, we employ the full-vectorial finite element method (FV-FEM). The basic equation to express the light propagating behavior in photonic devices is given as follows:

$$\nabla \times (p \nabla \times \Phi) - k_0^2 q \Phi = 0 \quad (8)$$

where k_0 is a free-space wavenumber, and p , q , and Φ are defined as follows:

$$\begin{cases} p = 1 & q = n^2 & \text{for } \Phi = \mathbf{E} \\ p = 1/n^2 & q = 1 & \text{for } \Phi = \mathbf{H} \end{cases} \quad (9)$$

where n is a refractive index distribution. Applying FV-FEM with tetrahedral edge element to (8), the following simultaneous linear equation is obtained [10]:

$$[P]\{\Phi\} = \{u\} \quad (10)$$

where $[P]$ is a FEM matrix and $\{u\}$ is a vector related to an incidence condition. Once the propagating field $\{\Phi\}$ is obtained, the scattering parameter from port 1 into port n is calculated as follows:

$$S_{n1} = \{g_n\}^T \{\Phi\} \quad (11)$$

where $\{g_n\}$ is the vector related to the modal field in port n .

2.3. Sensitivity analysis

2.3.1. Sensitivity analysis based on adjoint variable method

In order to optimize design variables, we have to evaluate sensitivity of device performance with respect to each design variables. For an in-plane structure in each layer, we employ the adjoint variable method (AVM) to efficiently evaluate the sensitivity and optimize the design variables by using the gradient descent method. The sensitivity of the scattering parameter S_{n1} with respect to $c_j^{(i)}$ is expressed as follows [11]:

$$\frac{\partial S_{n1}}{\partial c_j^{(i)}} = -\{\lambda_n\}^T \frac{\partial [P]}{\partial c_j^{(i)}} \{\Phi\} \quad (12)$$

where the adjoint variable $\{\lambda_n\}$ is calculated by

$$[P]^T \{\lambda_n\} = \{g_n\}. \quad (13)$$

Once we get $\{\lambda_n\}$, we can efficiently estimate sensitivity of each design parameter.

Here, in order to derive $\partial[P]/\partial c_j^{(i)}$, the derivative of the relative permittivity has to be required and is expressed as follows:

$$\frac{\partial \varepsilon_r}{\partial c_j^{(i)}} = f_j(x, z) (\varepsilon_{rb} - \varepsilon_{ra}) L_{di} \quad (14)$$

$$L_{di} = L_{d1} + \sum_{k=2}^i \left(H(w_k) + (1 - L_{k-1}) \frac{\partial H(w_k)}{\partial w_k} \right) \quad (i \geq 2) \quad (15)$$

$$L_{d1} = \frac{\partial H(w_1)}{\partial w_1}. \quad (16)$$

Using the sensitivities, design variables are updated as follows:

$$c_j^{(i)} = c_j^{(i)} + \delta_c \times (-\nabla_{c_j^{(i)}} C) \quad (17)$$

where $\nabla_{c_j^{(i)}} C$ is the gradient of the objective function with respect to the design variables and δ_c is the mobility of the design variables.

2.3.2. Sensitivity analysis for layer thickness

Although AVM is also possible to be utilized to evaluate the sensitivity of S_{n1} to the layer thickness, the gray area is required along the depth direction and the device performance is more sensitive to the structural deviation from the binarized device structure in the depth direction. Therefore, in this optimization, we employ the forward difference method instead of AVM for the sensitivity analysis with respect to the layer thickness because the number of design variables is small in the depth direction and only one variable is required to design two-layered structure. In the optimization process, the layer thickness is updated as follows:

$$h'_i = h_i + \delta_h \times \frac{|S_{n1}(h_i + \Delta h)|^2 - |S_{n1}(h_i)|^2}{\Delta h} \quad (18)$$

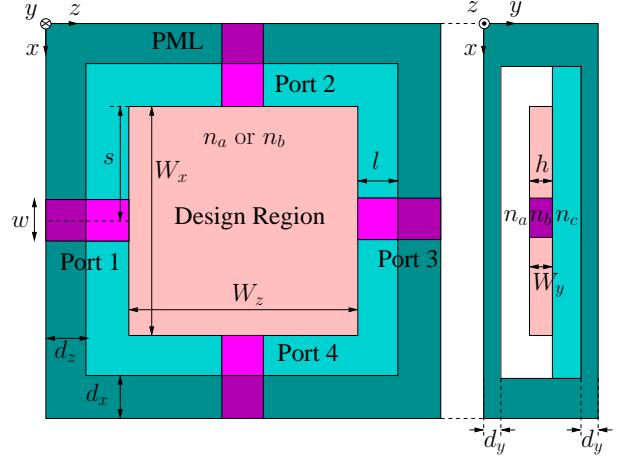


Figure 3: Design model of waveguide Crossing.

where Δh_i is the difference interval and δ_h is the mobility of the design variables of layer thickness.

3. Design examples

In this section, we show optimal design examples of optical waveguide devices using the optimization method described in the previous section.

3.1. Crossing waveguide

We consider a crossing waveguide as shown in Fig. 3. In this optimization, we impose a symmetry condition in the x and z directions and a 90 degree rotational symmetry condition so that the output characteristics in through and cross ports are equal for incidence to any port. The structural parameters are let to be $w = 500$ nm, $h = 220$ nm, $W_x = W_z = 3$ μ m, $W_y = 220$ nm, $s = 1.5$ μ m, $l = 0.5$ μ m, $d_x = d_z = 0.5$ μ m, and $d_y = 0.2$ μ m. The refractive indices of the materials are assumed to be $n_a = 1$, $n_b = 3.4$ and $n_c = 1.45$. The objective function to be minimized is given as follows:

$$\text{minimize } C = (1 - |S_{31}(\lambda_i)|^2)^2 \quad (i = 1, 2, 3). \quad (19)$$

In this design, in order to achieve desired property within the optical C-band, the wavelengths considered in (19) are set to be $\lambda_1 = 1.530$, $\lambda_2 = 1.550$, and $\lambda_3 = 1.565$ μ m. In the iteration process, these wavelengths are cyclically considered in (19). In order to obtain smooth convergence of optimization, it may be effective to use an objective function in which three wavelengths are simultaneously considered. On the other hand, optimization search is sometimes trapped around local minimum in some optimization problems with multiple-peak. In order to escape from a local minimum, some kind of randomness is sometimes effective. Therefore, we use cyclic strategy in this optimization process expecting that a trapping around a local minimum at one wavelength is solved when the other wavelength is considered. In addition, it is reported

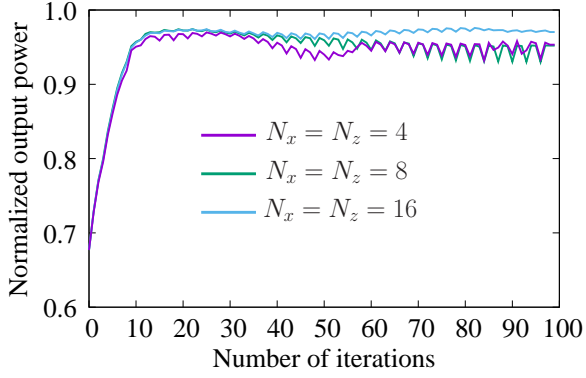


Figure 4: Output characteristics during the optimization process in the design of a waveguide crossing.

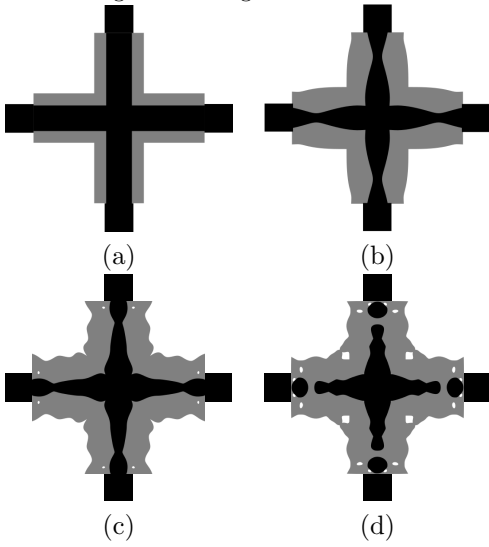


Figure 5: Initial structure and optimized structure with different numbers of expansion terms in optimization. (a) initial structure, (b) $N_x = N_z = 4$, (c) $N_x = N_z = 8$, (d) $N_x = N_z = 16$.

that, by aiming wideband operation, complex fine structures which are often appeared in the topology optimization can be suppressed to some extent[13]. Here, two layered structure is considered so as to obtain a low loss and low crosstalk device as shown in [14] and the thickness of lower and upper layers are set to be $h_1 = h_2 = 110$ nm in an initial structure. The maximum core height is fixed to $h = h_1 + h_2 = 220$ nm. Each parameter in equation (18) is set to be $\delta = 0.01$, $h = 1$ nm. In this study, aiming for achieving smaller crossing waveguide, the design region size is reduced to a quarter of the crossing in [14]. Figure 4 shows the improvement of the objective function in the optimization process. In this optimization, single iteration with FEM analysis and sensitivity analysis takes about 17 minutes using our handmade solver[10] and PC with an Intel Xeon CPU X5650 (2.67 GHz). The required computer memory is about 28 Gbyte. In this design example, Fourier series is employed as a structure definition function, $w_i(x, z)$ and the number of expansion terms are same in both layers and set to $N_x = N_z = 4, 8, \text{ or } 16$.

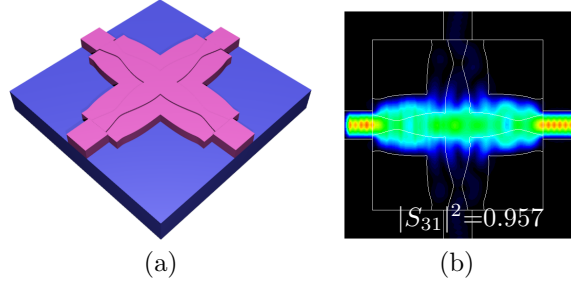


Figure 6: Optimization results of waveguide crossing at wavelength of $1.55 \mu\text{m}$. (a) 3D structure. (b) propagating field.

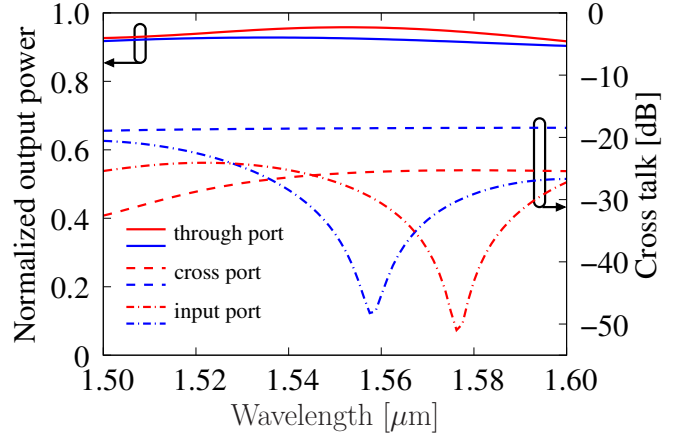
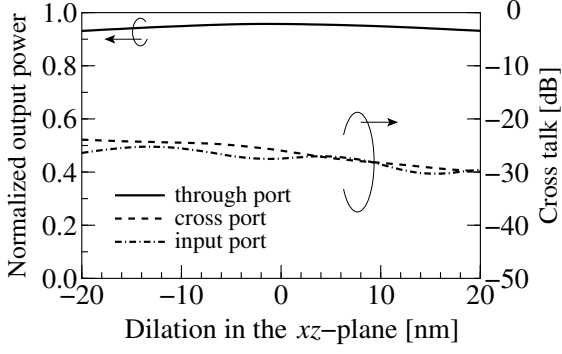
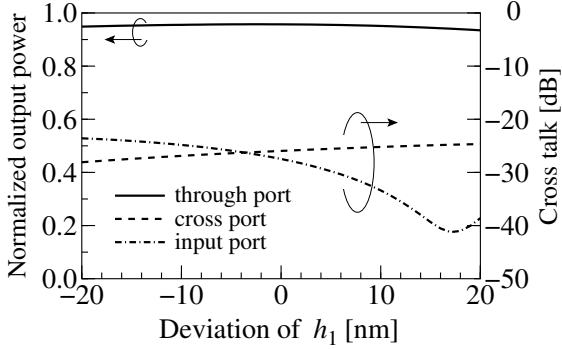


Figure 7: Wavelength dependence of the optimized waveguide crossing. Optimized layer thickness(red line) and fixed layer thickness(blue line).

16. The layer thicknesses are $(h_1, h_2) = (30 \text{ nm}, 190 \text{ nm}), (43 \text{ nm}, 177 \text{ nm}), (40 \text{ nm}, 180 \text{ nm})$ for $N_x = N_z = 4, 8, \text{ or } 16$, respectively. Although it is seen that the values of objective function are oscillating, this is because the considered wavelength is cyclically changed in this design. This treatment is sometimes effective to escape from local optima. Figure 5 shows the initial structure used in this optimization and the optimized device structures. The upper layer is drawn in black and lower layer is shown in gray. Although the transmittance in the optimized device with $N_x = N_z = 16$ is slightly higher than the other optimized device with fewer degree-of-freedom, the device structure is considerably complicated compared with the other ones. In the view of actual fabrication, we employ the optimized device with $N_x = N_z = 4$ and evaluate a wavelength dependence of this device. Figure 6 shows the optimized device structures and the propagating fields at wavelength of $\lambda = 1.55 \mu\text{m}$ and Fig. 7 shows the wavelength dependence of the transmittance and crosstalk in the optimized device. In order to show the effectiveness of this optimization with tunable layer thickness, the results obtained by the conventional optimization with fixed layer thickness are also shown. Here, in the conventional approach, layer thicknesses are fixed to $h_1 = h_2 = 110$ nm. It is seen that higher transmittance (≥ 0.916) and lower crosstalk (≤ -24 dB) while wavelength of $1.50 \mu\text{m}$ to $1.60 \mu\text{m}$ are obtained in



(a)



(b)

Figure 8: Structural tolerance of the optimized crossing waveguide as shown in Fig. 6 when wavelength is $\lambda_1 = 1.55 \mu\text{m}$. (a) dilation in the xz -plane, (b) deviation of h_1 .

this optimization compared with those obtained in the conventional one.

Finally, in order to check the structural tolerance of the designed crossing waveguide, we calculate the transmission property when the device structure is deviated from the optimized one. Figure 8 shows structural tolerance of the designed crossing waveguide ($N_x = N_z = 4$) for a structural deviation in the xz -plane and a deviation of the upper layer thickness, h_1 , respectively. In the case of the structural tolerance in the xz -plane, the core region is uniformly dilated or eroded in the normal direction to the material boundary. In the case of the tolerance to the layer thickness, the total core height $h = h_1 + h_2$ is fixed to 220 nm, thus, h_2 decreases when h_1 increases. In both cases, relatively high transmission and low cross talk are maintained within 20 nm structural deviation due to the relatively simple optimized device structure.

3.2. Polarization rotator and splitter

As a design example of polarization coupling device, we consider a design example of PSR. In order to realize polarization conversion, structural asymmetry along the depth direction has to be required and layered structure considered here is thought to be effective.

In this optimization, we consider the design model as shown in Fig. 9. The structural parameters are let to be $w = 0.4 \mu\text{m}$, $h = 0.3 \mu\text{m}$, $l = 0.5 \mu\text{m}$, $W_x = 3 \mu\text{m}$, $W_y =$

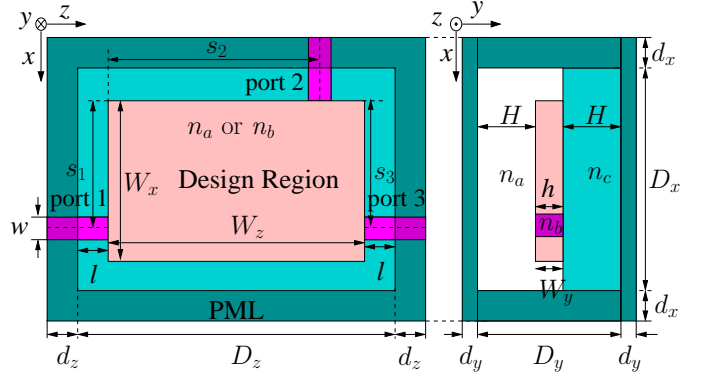


Figure 9: Design model of PSR.

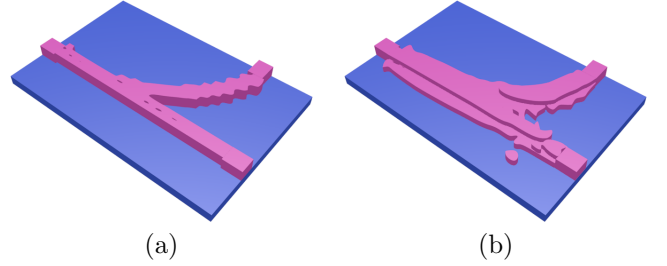
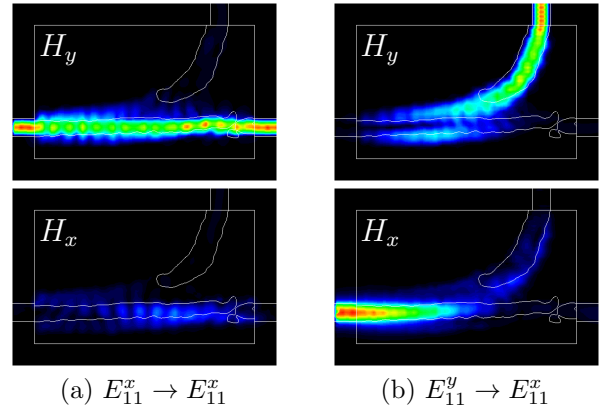


Figure 10: (a) Initial structure, (b) optimized structure.



(a) $E_{11}^x \rightarrow E_{11}^x$ (b) $E_{11}^y \rightarrow E_{11}^x$

Figure 11: Propagating field in the optimized PSR.

$0.3 \mu\text{m}$, $W_z = 5 \mu\text{m}$, $s_1 = s_3 = 2.3 \mu\text{m}$, $s_2 = 4.2 \mu\text{m}$, $L_x = 4 \mu\text{m}$, $L_y = 1.3 \mu\text{m}$, $L_z = 6 \mu\text{m}$, $H = 0.5 \mu\text{m}$, $d_x = d_z = 0.5 \mu\text{m}$, and $d_y = 0.2 \mu\text{m}$. The refractive indices of the materials are assumed to be $n_a = 1$, $n_b = 3.4$ and $n_c = 1.45$. We design a PSR which can split E_{11}^x and E_{11}^y modes launched from port 1 into port 2 and port 3, respectively, and convert E_{11}^y mode into E_{11}^x mode. The objective function to be minimized is given as follows:

$$\text{Minimize } C = \begin{cases} \left(1 - |S_{31}^{E_{11}^x \rightarrow E_{11}^x}|^2\right)^2 & (E_{11}^x \text{ incidence}) \\ \left(1 - |S_{21}^{E_{11}^y \rightarrow E_{11}^x}|^2\right)^2 & (E_{11}^y \text{ incidence}). \end{cases} \quad (20)$$

The incident wavelength is set to $1.55 \mu\text{m}$ and the number of expansion terms is set to $N_x = N_z = 16$. In order to suppress the appearance of complicated structure, we

Table 1: Comparison of several silicon-based PSRs

Device	Size [μm]	Loss [dB]	ER [dB]	B [nm]	Fabrication process
Ref.[20]	47.5	< 0.57	> 20	85	Single-Etching
Ref.[21]	27	< 0.5	> 20	20	Double-Etching
Ref.[22]	8.77	< 1	> 18	41	Double-Etching
Ref.[23]	70	< 0.5	> 20	50	Single-Etching
Ref.[24]*	> 80	0.09	> 30	160	Double-Etching
Ref.[25]*	> 10	> 0.11	> 19	O-band	Double-Etching
Our work*	6.0	< 1	> 20	160	Double-Etching

Size : Device length, ER : Extinction ratio, B : Bandwidth

*: Simulation

apply the Gaussian filter [12] in the optimization process.

Figure 10 shows the initial structure and optimized structure, where $h_1 = 133$ nm and $h_2 = 167$ nm. Figure 11 shows the propagating field in the optimized PSR. The normalized output power and polarization extinction ratio are $0.953(E_{11}^x \rightarrow E_{11}^x)$, 31.0 dB in port 3 and $0.960(E_{11}^y \rightarrow E_{11}^y)$, 30.7 dB in port 2, respectively, thus the desired operation of PSR is realized. In the case that the layer thickness is fixed, the transmittance for x-polarized light incidence is not sufficiently improved in this optimization process. On the other hand, in the present approach where layer thickness is optimized, the transmittance is well improved, for both polarization incidences. Figure 12 shows the improvement of the transmission and polarization rotation properties in the optimization process. The device performance is rapidly improved by about 100 iteration steps. The slight degradation of the device performance in the last part of the iteration is due to the effect of structural smoothing[12]. Although, in order to improve convergence behavior, it may be effective to relax the structural smoothing effect during the optimization process, overrelaxation may produce complex fine structures. To improve our design approach into perfectly balanced optimization between device performance improvement and structural smoothing is our future work. In this optimization, single iteration with FEM analysis and sensitivity analysis takes about 13 minutes using our handmade solver[10] and PC with an Intel Xeon CPU X5650 (2.67 GHz). The required computer memory is about 25 Gbyte. Figure 13 shows the wavelength dependence of the optimized structure. It is seen that the insertion loss of less than 1 dB and the extinction ratio of higher than 20 dB are achieved from a wavelength of $1.45 \mu\text{m}$ to $1.60 \mu\text{m}$, so the PSR that can operate in a wide wavelength band can be designed. Table 1 shows a comparison of the properties of the designed PSR and previously reported ones. Considering that the footprint of the functional area is $3 \times 5 \mu\text{m}^2$, the PSR designed by our method is more compact and has higher performance than the PSRs reported previously [20–25].

Finally, in order to check the structural tolerance of the designed PSR, we calculate the transmission property when the device structure is deviated from the optimized one. Figure 14 shows structural tolerance of the designed PSR for a deviation in the xz -plane and a deviation of

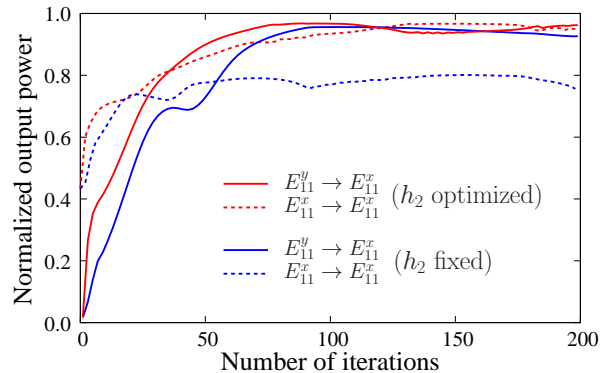


Figure 12: Output characteristics during the optimization process in the design of a PSR.

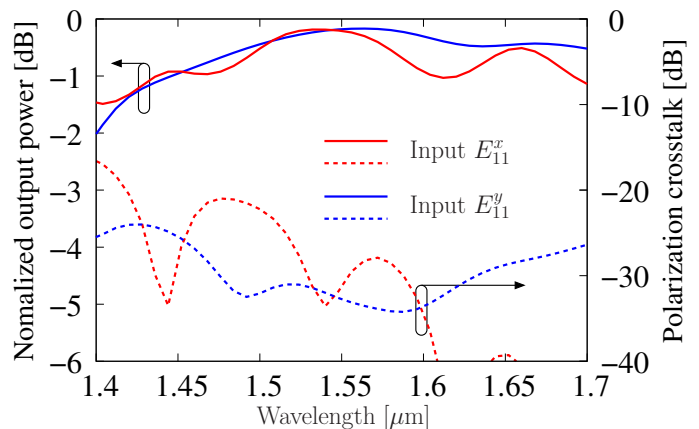


Figure 13: Wavelength dependence of the optimized PSR.

the upper layer thickness, h_1 , respectively. In the case of the structural tolerance in the xz -plane, the core region is uniformly dilated or eroded in the normal direction to the material boundary. In the case of the tolerance to the layer thickness, the total core height $h = h_1 + h_2$ is fixed to 300 nm, thus, h_2 decreases when h_1 increases. From these results, we can see that the device performance is more sensitive to the structural deviation in the xz -plane. Robust optimization considering a structural tolerance is our future work.

4. Conclusion

In this paper, we proposed an optimal design method to design three dimensional optical waveguide devices with layered structure by using function-expansion-based topology optimization. As design examples, a crossing waveguide and PSR with layered structure were designed to show the validity and usefulness of our approach. In this newly improved design approach, the floating structure which is hard to fabricate, is not essentially generated. In the design example, it was shown that the device performance can be further improved by optimizing layer thickness. We

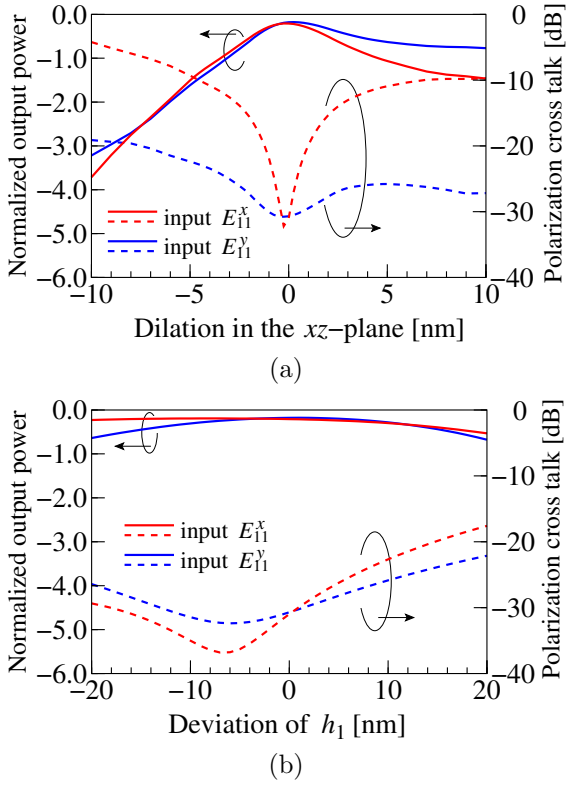


Figure 14: Structural tolerance of the optimized PSR as shown in Fig. 10(b). (a) dilation in the xz -plane. (b) deviation of h_1 .

will apply this approach to design problems of various compact and high performance photonic devices required in the future photonic network.

Acknowledgement

This work was supported by JSPS KAKENHI Grant Number 18K04276.

References

- [1] J. Lu and J. Vučković, Objective-first design of high-efficiency, small-footprint couplers between arbitrary nanophotonic waveguide modes, *Opt. Express*, 20 (7) (2012) 7221–7236.
- [2] L. H. Frandsen, Y. Elesin, L. F. Frellsen, M. Mitrovic, Y. Ding, O. Sigmund, and K. Yvind, Topology optimized mode conversion in a photonic crystal waveguide fabricated in silicon-on-insulator material, *Opt. Express* 22 (7) (2014) 8525–8532.
- [3] J. Huang, J. Yang, D. Chen, X. He, Y. Han, J. Zhang, and Z. Zhang, Ultra-compact broadband polarization beam splitter with strong expansibility, *Photon. Res.* 6 (6) (2018) 574–578.
- [4] A. Iguchi, Y. Tsuji, T. Yasui, and K. Hirayama, Efficient topology optimization of optical waveguide devices utilizing semi-vectorial finite-difference beam propagation method, *Opt. Express* 25 (23) (2017) 28210–28222.
- [5] Z. Yu, H. Cui, and X. Sun, Genetic-algorithm-optimized wide-band on-chip polarization rotator with an ultrasmall footprint, *Opt. Lett.*, 42, (16) (2017) 3093–3096.
- [6] J. L. Pita, I. Aldaya, P. Dainese, H. E. Hernandez-Figueroa, and L. H. Gabrielli, Design of a compact CMOS-compatible photonic antenna by topological optimization, *Opt. Express*, 26 (3) (2018) 2435–2442.

- [7] K. Mori, K. Morimoto, T. Tanaka, A. Iguchi, and Y. Tsuji, Topology optimization of nonlinear optical waveguide devices considering output signal phase, *Opt. Commun.*, 439 (2019) 290–294.
- [8] H. Han, H. Li, X. Zhang, A. Liu, T. Lin, Z. Chen, H. Lv, M. Lu, X. Liu, and Yan-Feng Chen, High performance ultra-compact SOI waveguide crossing, *Opt. Express*, 26 (20) (2018) 25602–25610.
- [9] Y. Tsuji and K. Hirayama, Design of optical circuit devices using topology optimization method with function-expansion-based refractive index distribution, *IEEE Photon. Technol. Lett.*, 20 (12) 2008 982–984.
- [10] T. Yasui, Y. Tsuji, J. Sugisaka, and K. Hirayama, Design of three-dimensional optical circuit devices by using topology optimization method with function-expansion-based refractive index distribution, *J. Lightw. Technol.* 31 (23) (2013) 3765–3770.
- [11] Z. Zhang, Y. Tsuji, T. Yasui, and K. Hirayama, Design of ultra-compact triplexer with function-expansion based topology optimization, *Opt. Express*, 23 (4) (2015) 3936–3950.
- [12] H. Goto, Y. Tsuji, T. Yasui, and K. Hirayama, A study on optimization of waveguide dispersion property using function expansion based topology optimization method, *IEICE Trans. Electron.*, E97-C (7) (2014) 670–676.
- [13] K. Fujimoto, Y. Tsuji, K. Hirayama, T. Yasui, S. Sato, and R. Kijima, A study on topology optimization of optical circuits consisting of multi-materials, *J. Lightw. Technol.*, 30 (13) (2012) 2210–2215.
- [14] W. Bogaerts, P. Dumon, D. V. Thourhout, and R. Baets, Low-loss, low-cross-talk crossings for silicon-on-insulator nanophotonic waveguides, *Opt. Lett.*, 32 (19) (2007) 2801–2803.
- [15] M. Aamer, A. M. Gutierrez, A. Brimont, D. Vermeulen, G. Roelkens, J. Fedeli, A. Håkansson, and P. Sanchis, CMOS compatible Silicon-on-Insulator polarization rotator based on symmetry breaking of the waveguide cross section, *IEEE Photon. Technol. Lett.*, 24 (22) (2012) 2031–2034.
- [16] B. Kumari, R. K. Varshney, and B. P. Pal, Design of a promising silicon slot waveguide-based ultra-short low loss efficient polarization rotator for the mid-IR, *Optik*, 180 (2019) 71–83.
- [17] X. Sun, J. S. Aitchison, and M. Mojahedi, Realization of an ultra-compact polarization beam splitter using asymmetric MMI based on silicon nitride / silicon-on-insulator platform, *Opt. Express*, 25 (7) (2017) 8296–8305.
- [18] Q. Fang, X. Chen, Y. Zhao, J. Hu, H. Chen, C. Qiu, and M. Yu, Folded Silicon-Photonics arrayed waveguide grating integrated With loop-mirror reflectors, *IEEE Photon. J.*, 10 (4) (2018).
- [19] S. Tomioka, T. Tanaka, K. Mori, Y. Tsuji, Design of polarization splitter and rotator using function-expansion based topology optimization considering two-layer structure, *JASSE*, 6 (1) (2019) 141–148.
- [20] H. Xu and Y. Shi, Ultra-broadband silicon polarization splitter-rotator based on the multi-mode waveguide, *Opt. Express*, 25 (15) (2017) 18485–18491.
- [21] H. Guan, A. Novack, M. Streshinsky, R. Shi, Q. Fang, A. E. Lim, G. Lo, T. Baehr-Jones, and M. Hochberg, CMOS-compatible highly efficient polarization splitter and rotator based on a double-etched directional coupler, *Opt. Express*, 22 (3) (2014) 2489–2496.
- [22] Y. Zhang, Y. He, X. Jiang, B. Liu, C. Qiu, Y. Su, and R. A. Soref, Ultra-compact and highly efficient silicon polarization splitter and rotator, *APL Photonics*, 1 (9) (2016) 91304.
- [23] D. Dai and H. Wu, Realization of a compact polarization splitter-rotator on silicon, *Opt. Lett.*, 41 (10) (2016) 2346–2349.
- [24] Y. Xiong, D.-X. Xu, J. H. Schmid, P. Cheben, S. Janz, and W. N. Ye, Fabrication tolerant and broadband polarization splitter and rotator based on a taper-etched directional coupler, *Opt. Express*, 22 (14) (2014) 17458–17465.
- [25] K. Tan, Y. Huang, G.-Q. Lo, C. Lee, and C. Yu, Compact highly-efficient polarization splitter and rotator based on 90° bends, *Opt. Express*, 24 (13) (2016) 14506–14512.